HHS Public Access

Author manuscript

J Orthop Res. Author manuscript; available in PMC 2018 February 01.

Published in final edited form as:

J Orthop Res. 2017 February ; 35(2): 353–360. doi:10.1002/jor.23285.

Kinematics of Meniscal- and ACL-Transected Mouse Knees during Controlled Tibial Compressive Loading Captured using Roentgen Stereophotogrammetry

Olufunmilayo O. Adebayo, M.S.[1], **Frank C. Ko, Ph.D.**[2], **Steven R. Goldring, M.D.**[3], **Mary B. Goldring, Ph.D.**[3], **Timothy M. Wright, Ph.D.**[3], and **Marjolein C.H. van der Meulen, Ph.D.**[1,2,3]

[1]Meinig School of Biomedical Engineering, Cornell University, Ithaca, NY

[2]Sibley School of Mechanical and Aerospace Engineering, Cornell University, Ithaca, NY

[3]Research Division, Hospital for Special Surgery, New York, NY

Abstract

Pre-clinical studies of post-traumatic OA have examined the pathways that lead to disease after injury by using surgical models such as the destabilization of the medial meniscus (DMM) and anterior cruciate ligament transection (ACLT). While the morphological, molecular and genetic pathways leading to OA have been examined extensively; the effects of these injuries on joint kinematics, and thus disease progression, have yet to be fully characterized. To this end, we sought to understand the kinematics in the DMM and ACLT joints compared to intact joints subjected to controlled tibial compressive loading. We hypothesized that the DMM and ACLT models would result in different patterns of joint instability compared to intact joints, thus explaining the different patterns of OA initiation and severity in these models. Cadaver adult C57BL/6 mice were subjected to either a DMM or ACLT in their right knee joints, while the left limbs remained as intact controls. All limbs were labeled with fiducial markers, and the rigid body kinematics of the tibia and femur were examined using roentgen stereophotogrammetry (RSA) with application of compressive loads from 0 to 9N. DMM and intact joints demonstrated similar kinematics under compressive loading, in contrast to ACLT joints, which dislocated even before load application. These results demonstrate the importance of rigorous kinematic analysis in defining the role of joint instability in animal models of OA and suggest significant differences in DMM and ACLT joint instabilities in the context of controlled mechanical loading.

Keywords

kinematics; knee; osteoarthritis; anterior cruciate ligament; destabilization of the medial meniscus

Corresponding Author: Marjolein C.H. van der Meulen, Ph.D., Meinig School of Biomedical Engineering, Cornell University, 113 Weill Hall, Ithaca NY 14853, Tel: (607)-255-1445, Fax: (607)-255-1222, mcv3@cornell.edu.

Author Contributions:

Concept and design: OOA, FCK, SRG, MBG, TMW, MCHM

Acquisition, analysis and interpretation of the data: OOA, FCK, SRG, MBG, TMW, MCHM

Drafting and critical revision of the article: OOA, FCK, SRG, MBG, TMW, MCHM

Final approval of the article: OOA, FCK, SRG, MBG, TMW, MCHM

Introduction

Osteoarthritis (OA) is characterized clinically by cartilage degradation, subchondral bone changes, joint pain and impaired joint function[1, 2]. Tissue alterations in OA joints extend beyond cartilage and bone to include changes in the menisci, ligaments and other peri-articular soft tissues[3]. Epidemiological studies indicate that abnormal biomechanical loading and joint instability from injury are important etiological factors in the pathogenesis of OA[1, 4]. This concept is substantiated by observations that certain occupational activities[5–7], obesity[8, 9], and joint laxity and injury[10–12] are correlated with an increased risk of OA, while reduction in body weight[13] and mild to moderate exercise[14, 15] may slow disease progression. Although epidemiological and clinical studies of OA suggest a strong relationship between the joint mechanical environment and the incidence of the disease, the exact ways in which changes in the mechanical environment influence OA initiation and progression are not well defined[16].

Pre-clinical studies in murine species using surgical models, such as the destabilization of the medial meniscus (DMM)[17, 18] and anterior cruciate ligament transection (ACLT)[17, 19], have examined the structural changes and biological pathways that lead to OA disease initiation after joint injury. These models induce moderate to severe OA pathology characterized by cartilage degradation and subchondral bone changes, and provide insights into the morphological and biochemical changes in joint tissues during OA disease progression[17–20]. Furthermore, while several studies demonstrated that these injuries affect joint stability in large vertebrates[21–24], the relationship between altered joint kinematics and the initiation of OA has not been fully characterized in murine models due to their small size. Measurements of joint kinematics in murine models have been limited to using weight bearing and ground reaction forces as metrics for instability[25, 26]. While these data provide information on the functionality of the joint, they do not describe joint instability or the mechanical environment associated with the injury. Thus, these studies have provided little insight into how these joint injuries affect joint stability and how the altered joint kinematics relates to OA initiation. Characterization of joint kinematics in the DMM and ACLT models would provide valuable insights into the influence of instability on the local mechanical environment during the initiation and progression of OA, strengthening their use as small-animal models of post-traumatic OA.

Our group and others have previously presented a non-invasive tibial loading model in mice for bone adaptation studies[27, 28]. The loading device in this model allows for normal flexion of the knee, while applying a controlled axial compressive load to the tibia through the femoral condyles. Adapted from the mouse ulna loading model[30], the tibial loading model has been used extensively in orthopaedics to study bone adaptation and is a widely accepted platform to recapitulate physiological mechanical forces during mouse gait[27–29], with a 9N compressive load creating 1200με at the mid-shaft of the tibia[29]. This strain value is well within the normal range of functional strains during locomotion in mice and most vertebrates[31–34]. Recently, our group and others used this model on intact joints to recapitulate major features of OA after 1, 2, and 6 weeks of loading[35–37], with similar results to those induced by long-term treadmill running in mice[38]. To date, however, the tibial compressive loading model has not been applied to DMM and ACLT injured mouse knees.

With the understanding that mechanical forces play a key role in OA, we aimed to characterize the effects of the joint injuries in the DMM and ACLT models on joint kinematics under loading conditions. We hypothesized that the DMM and ACLT models would alter stability compared to intact joints, thus enabling future experiments to explore the effects of joint instability on patterns of OA initiation and severity in these mouse models under controlled loading. Our loading device, which permits controlled application of compressive loads to the tibia, was used as a tool to quantify and compare joint kinematics of intact, DMM and ACLT joints under a controlled loading regime. Due to the orientation and range of motion of the knee under our loading conditions, our results directly measured bone kinematics, rather than joint kinematics. Our results provide insights into the effects of these joint injuries on bone kinematics and associated joint motions in the context of defined compressive loading and demonstrate the importance of rigorous kinematic analysis to better understand disease progression in murine models of OA.

Methods

Animal Models

Eight 32-week old freshly frozen C57BL/6 male mice (Jackson Laboratories, Bar Harbor, ME) were obtained and thawed at room temperature. The right knee joint of each mouse was subjected to either DMM or ACLT (n=4/group). Following previously established protocols[17], a longitudinal incision was performed from the distal patella to the proximal tibia. The joint capsule was exposed, and the fat pad was dissected, allowing visualization of the medial meniscotibial ligament (MMTL) and the anterior cruciate ligament (ACL). Using a #11 blade, either the MMTL or the ACL was transected. Care was taken to ensure that all other ligaments remained intact. The joint capsule was then closed with a continuous cutting suture (4-0 Sofsilk, Covidien, Minneapolis, MN). The left knee joints remained as intact controls.

Fiducial Marker Placement

To place the fiducial makers on the joint for use in kinematics measurements, two small incisions were created, one on the medial proximal region of each tibia and the other on the anterior distal region of each femur. The muscle and skin were retracted using blunt dissection techniques, and a periosteal elevator was used to remove the periosteum. The exposed bone was degreased with methyl ethyl ketone. At least 3 100μm tin/lead solder spheres (Caplinq Co., Ottawa ON, Canada) were affixed to a 2mm×2mm flexible adhesive plastic to serve as fiducial bone markers. The bone markers were adhered onto the exposed regions of the tibia and femur using cyanoacrylate. Care was taken to ensure that the markers adhered firmly to the bone, and that the joint capsule remained intact.

Mechanical Loading & Imaging Protocol

All limbs were loaded from 0 to 9N compression at 1N increments using the tibial compressive loading device[35] (Fig. 1A). The loading device is equipped with a feedback control loop (National Instruments, Labview v8.2) that allows the user to set a constant compressive force at each load step (Fig. 1B), using an in-line force transducer (ELPF-T2E-10L, Measurement Specialties). Medial-lateral radiographs were obtained at each

stepped load using a single dental x-ray (VetVision DC, Progeny Dental, Lincolnshire, IL), with a resolution of 28μm. The stepped loading protocol was then repeated to obtain anterior-posterior radiographs (Fig. 1C). This loading and imaging scheme was repeated for 3 trials per joint.

Compressive loading was applied through an actuator affixed to a foot-holder in the loading device, while the force transducer was attached to the knee-holder (Fig. 1A). With each progressive load step, the foot-holder applied compression through proximal translation along the X-axis, towards the knee joint (Fig. 1C). A prior kinematic analysis identified that this translation was associated with a slight positive rotation (1.4±1.3°) about the Z-axis at 9N. Thus, any positive rotations about the Z-axis resulting in adduction or abduction within this angular range were regarded as a function of the loading device for the right and left knee, respectively.

Roentgen Stereophotogrammetry

Roentgen stereophotogrammetry (RSA) examination was performed using a custom-made calibration cage and previously-established protocols [39–41]. The calibration cage consisted of 2 orthogonal planes, one for each x-ray position, containing sets of tantalum markers with known locations. One set of markers defined the 3D global fiducial coordinate system, while the other set was used to determine the exact location of the dental x-ray. Error analysis was performed on the system using a phantom consisting of 2 wooden rods (2.2mm diameter, 15cm length), each labeled with at least 4 fiducial markers. To measure both the precision and accuracy of the system, we conducted 9 double examinations of the phantom with no relative motion between rods, similar to previous protocols[40]. Radiographs were taken at the 2 planes of the calibration cage, and used to determine each fiducial marker location, rigid-body fitting, and subsequent calculation of motion.

The relative motion calculated by the RSA set-up for the 9 examinations was averaged as the error of the system, and the standard deviation of these motions was the precision. The error and precision (mean ± standard deviation) associated with zero motion of the phantom were 0.03±0.25mm, -0.01±0.08mm, and -0.16±0.37mm in translation along the X-, Y-, and Z-axes, respectively, and -0.9±2.2°, 0.8±1.4°, and 1.3±1.3° in rotation about the X-, Y-, and Z-axes, respectively. These values were interpreted as the systematic error associated with calculations of rigid body motion using this RSA set-up, and any motions within the bounds of our error values were deemed negligible.

Furthermore, the use of a single dental x-ray for imaging two planes introduced an inherent error in joint positioning because the loading protocols were performed sequentially. We defined this error as the average error in determining the exact 3D location of the fiducial markers. The position of each marker was calculated as the intersection between the position vectors from each imaging focus point. However, due to both a systematic error from the lack of exact alignment of the two orthogonal planes of the calibration cage, and the irreproducibility of the joint positioning with a sequential loading protocol, the position vectors did not intersect in 3D space. Therefore, the position of each bone marker was calculated as the midpoint of the shortest line connecting the two vectors, with the error defined as half the length of the line along each axis. Using data from a previous kinematic

analysis in which five mouse joints were placed under the same protocol for 15 loading/imaging protocols, we determined the average error of the system to be [±63μm, ±2.0μm, ±1.6μm] in the X-, Y- and Z-axes respectively.

Kinematics Analysis

All joints were placed in the loading device, with the tibial axis of loading aligned to the X-axis of the calibration cage (Fig. 1), and RSA examination was performed. First, the initial, non-loaded position of the joint was examined qualitatively in the loading device. Due to the small size of the mouse joint, a reliable and consistent femoral coordinate system could not be established, thus all motions were described as translation and rotation from 0N load around the 3 axes in a tibial-oriented coordinate system. In accordance with RSA techniques, the tibial coordinate system was based on a reference alignment of the bone position in the loading device at 0N. Specifically, the tibial X-axis was defined as the axis at 0N in which the compressive load was applied, running from the tarsus to the intercondylar eminence, and was aligned to the global X-axis. Furthermore, we assumed that the tibial Y-axis at the 0N position in the loading device intersected both the medial and lateral tibial plateaus, and was parallel to the global Y-axis. The tibial Z-axis, perpendicular to both the X- and Y-axes, thus paralleled the global Z-axis. To determine translation along each axis, the point of interest (POI) was defined as the geometric center of the tibial and femoral articulating surfaces for both the tibia and the femur (Fig. 2). The location of the POI was defined and digitized manually as the midpoint of the overlapping surface of the tibia and femur in the 0N medial-lateral radiograph and the intercondylar eminence of the tibia in the 0N anterior-posterior radiograph.

To describe joint motions, tibial motion was first calculated at each stepped load as translation of the point of interest and Eulerian rotation of the bone about the body-oriented X-Y-Z axes relative to its position at 0N. These motions were thus interpreted as inferior-superior (IS), medial-lateral (ML), and anterior-posterior (AP) translations of the tibial plateau, and internal-external (IE), flexion-extension (FE), and abduction-adduction (AA) rotation of the tibia. Then, the relative femur-to-tibia motion, interpreted as the motion of the knee joint, was determined using the tibia as the reference segment. Specifically, the motion of the tibia at each stepped load was first transformed back to its position at 0N, and then the relative motion of the femur was calculated in the tibial coordinate system. Relative translation in this case was calculated as the difference in the position of the point of interest due to femoral versus tibial motion from 0N to each stepped load. All coordinate system creations and kinematics calculations were completed in Matlab using a custom-written code.

Statistics

Statistical analysis was performed to compare the kinematics of intact and ligament-transected joints. All intact joints from both DMM and ACLT groups were pooled for statistical analysis with the exception of one intact joint that was dislocated due to an accidental initial overload in the loading device. The results of the kinematics trials for each joint were averaged and represented as descriptive data for statistical analysis. Due to the small sample size of each group, a Kruskal-Wallis test was then performed to compare the

kinematics of intact and injured joints at each stepped load (JMP Pro 10.0, SAS Institute Inc). All data are shown as mean ± standard deviation, unless otherwise indicated. p-values of <0.05 indicate significance.

Results

Comparison of Joint Positions in the Loading Device

Changes in the joint position in the loading device were evident between the two models, even before the application of any compressive load (Fig. 3). The DMM joints maintained positions similar to those of the intact joints in the loading device, with an apparent articulating surface between the femur and tibia. However, all of the ACLT joints dislocated when placed in the loading device, even without compressive load. The dislocation resulted in the loss of an articulating surface between the femur and tibia, and thus further analysis of bone kinematics could not be performed accurately.

Tibial Motion Under Compression

The tibial motions of intact and DMM joints were similar at each stepped load relative to 0N. As the compressive load increased from 0 to 9N, both intact and DMM tibias exhibited superior translation, which peaked at 0.3±0.1mm and 0.2±0.0mm at 9N, respectively (Fig. 4A). Additionally, both groups demonstrated minimal translation along the ML axis and AP motion of the tibia, which peaked at similar values for both intact and DMM joints (Figs. 4B-C). None of the translational motions of the tibia were significantly different at any of the loads ($p = 0.13 – 0.85$). IE rotation was also minimal ($p = 0.19 – 0.85$) in all intact and DMM tibias, and the degree of tibial flexion was not different ($p = 0.45 – 1.0$) between intact and DMM groups (Figs. 4D-E). In contrast, the degree of tibial adduction at loads ≥ 4N was significantly different between the two groups ($p<0.04$, Fig. 4F), although the differences were small (tibial adduction of 1.5±0.7° at 9N in intact joints and tibial abduction of 1.7±0.6° in DMM joints).

Knee Joint Motion (Relative Femur to Tibia Motion) under Compression

Femur-to-tibia translations were minimal along the SI and AP axes (Figs. 5A,C). However, ML translation of the femur to tibia was significantly different between intact and DMM joints at 8N and 9N loads ($p < 0.01$, Fig. 5B). Intact joints exhibited little motion (0.1±0.1mm) along the ML axis; however, in DMM joints, we observed lateral translation of the femur starting at 6N, which peaked at 0.2±0.1mm at the 9N load. In both DMM and intact joints, we observed minimal internal rotation and similar flexion of the femur at most loads (Figs. 5D-E). However, rotation about the tibial AP axis was significantly different between these groups with femoral abduction (with the knee moving into varus) occurring in DMM joints compared to intact joints at all compressive loads ($p = 0.0082$, Fig. 5F).

Discussion

While pre-clinical models, such as DMM and ACLT, recapitulate features of post-traumatic OA[17–20], the exact mechanical environment associated with disease initiation and progression in these models is not understood completely. We sought to determine the

kinematics of DMM and ACLT joints under a controlled loading environment, to gain insights into the impact of the injuries on joint stability. Our results demonstrate that bone kinematics and, by extension, joint instability depend on the type of destabilization injury. Specifically, the initial dislocation of ACLT joints within the loading device, which allows for normal flexion, and the apparent loss of contact surface between the tibia and femur indicate that ACLT models of OA exhibit high levels of instability, with loading occurring at the edge of the injured joint[42]. In contrast, most measures of tibial and femoral motion were similar between DMM and intact joints, with only subtle differences in frontal plane rotations of the tibia and femur and greater relative lateral translation of the femur at higher compressive loads. While the differences in frontal rotations were significant, these small positive rotations about the AP-axis were within the range of the inherent motion of the foot-holder. Thus, the only significant, relevant difference between DMM and intact joints was in the slight lateral translation of the femur in the DMM group. Such similarities between kinematics in DMM and intact joints suggest that the induction of OA-like features in the DMM mouse model may not be due necessarily to extreme joint instability, but rather to a change in contact stresses as a result of an abnormal contact area[43–45].

Our study provides novel information about kinematics and instability of ACLT joints, specifically in murine models of OA, and such results are similar to those reported in other cadaveric studies. Bedi and colleagues reported kinematic changes in cadaveric human knees after an ACL injury, with significantly increased contract stress in the posterior-central aspect of the tibial plateau[46]. This finding is supported by other studies in mice, rabbits, sheep and humans, and is due to the increased anterior translation of the tibia as a result of the lack of the stabilizing constraint provided by the ACL[19, 21, 47–49]. In our study, the increased anterior translation of the tibia resulted in dislocation of the joint within the loading device, which may explain the rapid rate of OA progression present in murine ACLT models. *In vivo* murine joints subjected to ACLT demonstrate tibial anterior subluxation, marked degradation of the posterior aspect of the tibial cartilage, erosion of the tibial posterior subchondral bone, and osteophyte formation at the joint margins[17, 19]. These *in vivo* results indicate the presence of high joint instability and an abnormal anterior translation of the tibia during gait, consistent with the ACLT causing extreme joint motions, even in an otherwise well-controlled animal study[47]. While the ACLT mouse model is a relevant model of post-traumatic OA to understand pathologic joint tissue changes associated with such injuries, the kinematics of the model are extreme in the mouse. Thus, ACLT is unsuitable for mouse studies focused on elucidating the relationship between kinematics and subsequent joint injury and OA initiation.

To our knowledge, our study is the first to present the kinematics of DMM rodent joints under controlled mechanical loading. A previous study conducted by Allen and colleagues[25] focused on weight-bearing limb measurements in rats with medial collateral ligament (MCL) and medial meniscal transections, two more severe joint destabilization models. Significant differences were present in gait dynamics between injured and normal joints[25]. In contrast, our results suggest that the joint kinematics are generally unaffected by the DMM injury, which is much less destructive than a complete MCL or medial meniscal transection. Although we did not examine *in vivo* dynamic kinematics, our results are further substantiated by the slower rate of OA progression in DMM models compared to ACLT

models *in vivo*[17, 19, 50]. Indeed, the progression of moderate OA in DMM and other meniscal injury situations has been attributed to the disruption of tibiofemoral contact mechanics, with damage to the meniscus causing decreased cartilage contact area[43–45, 51]. Thus, higher stresses occur in the cartilage, particularly over the medial aspect of the tibia[17, 50, 52]. Although both the ACLT and the DMM mouse models develop OA-like features, the results of this study, along with evidence from *in vivo* studies, suggest that the joint mechanical environment associated with disease initiation differ. The DMM model reflects increased contact stress due to a reduction of contact area. In contrast, the ACLT model resulted in tibial dislocation under normal flexion, suggesting extreme loading between any remaining articulating surfaces due to the injury compared to the DMM model. This finding, though obtained *ex vivo*, is supported by *in vivo* evidence, and leads to the likely conclusion that with tibial compressive loading during mouse gait, these differences in mechanical environment may play at least a partial role in the severity and progression of OA *in vivo*[53].

Our study has limitations. While we used a controlled mechanical platform to examine the kinematics of ACLT and DMM joints, strict axial compression of the tibia through the femoral condyles may not elicit the same motions that occur during gait. However, our intention was to examine bone kinematics using a controlled loading model that generates physiological mid-shaft strains and that recapitulates OA features[35]. This model induces OA by superimposing short cycles of controlled tibial loading over otherwise normal cage activity, and without the surgical disruption of the joint[35, 36]. In contrast, DMM and ACLT models require invasive surgery, which induces inflammation that, in itself, may cause abnormal alterations in bone kinematics, thus confounding interpretation of the results. The compressive loading used in our study was done with little external constraint to the knee; the joint surfaces were free to move in any direction, though the motions of the tibia and femur were somewhat constrained to flexion-extension by the manner in which the tibia and femur were held in the loading fixture (Fig. 1A). Furthermore, the applied loads were small and controlled compared to those applied by muscles and ligaments during normal cage activity. In addition, our approach did not account for tissue adaptation and muscle forces that may play a role *in vivo*. Nonetheless, we showed striking differences in bone kinematics following DMM and ACLT, even when our relatively mild loading regime was applied. These differences in bone kinematics are likely exacerbated during normal cage activity, which may explain the differences in initiation and progression of OA pathology in the two models.

Additional considerations for our study are the use of a tibial-based coordinate system to describe knee joint kinematics, the small sample sizes, and the use of incremental static measurements of kinematics *ex vivo*. However, these points are offset by the fact that our study is the first to quantitatively characterize the bone kinematics associated with ACLT and DMM injuries in mice under controlled physiological tibial compressive loading. Thus, our results provide valuable insight into understanding the joint instability associated with these two commonly used OA mouse models *in vivo*.

In conclusion, we found marked differences in bone kinematics in the DMM and ACLT joints under controlled loading conditions. ACLT knees have extreme joint instability, which

may explain the rapid progression of OA, particularly in the posterior aspect of the tibial plateau *in vivo*. In contrast, DMM joints exhibit kinematics similar to those in intact knees, suggesting that the progression of OA in this model reflects altered joint kinematics and contact mechanics, not a more extreme loading scenario. In summary, although both the ACLT and DMM mouse models have strengths and limitations with respect to elucidating the pathways associated with OA initiation and progression, the DMM model provides a more representative and relevant model of post-traumatic OA in terms of physiological bone kinematics.

Acknowledgments

The authors thank Dr. Cecilia Dragomir for her expertise and training in the ACLT and DMM surgeries, and the Cornell/HSS Biomechanics group and Cornell CARE staff for their experimental assistance. This work was supported by NIH R21-AR064034, the Robert & Helen Appel Fellowship, Clark and Kirby Foundations, NSF GRFP (OOA), and Sloan Graduate Fellowship (OOA).

References

1. Felson DT, Lawrence RC, Dieppe PA, et al. Osteoarthritis: New Insights. Part 1: The Disease and Its Risk Factors. Ann. Intern. Med. 2000; 133(8):635–646. [PubMed: 11033593]
2. Felson DT. Osteoarthritis of the knee. N. Engl. J. Med. 2006; 354(8):841–848. [PubMed: 16495396]
3. Martel-Pelletier J. Pathophysiology of osteoarthritis. Osteoarthr. Cartil. 2004; 12:31–33.
4. Goldring MB, Marcu KB. Cartilage homeostasis in health and rheumatic diseases. Arthritis Res. Ther. 2009; 11(3):224. [PubMed: 19519926]
5. Kaila-Kangas L, Arokoski J, Impivaara O, et al. Associations of hip osteoarthritis with history of recurrent exposure to manual handling of loads over 20 kg and work participation: a population-based study of men and women. Occup. Environ. Med. 2011; 68(10):734–738. [PubMed: 21245478]
6. Cameron KL, Hsiao MS, Owens BD, et al. Incidence of physician-diagnosed osteoarthritis among active duty United States military service members. Arthritis Rheum. 2011; 63(10):2974–2982. [PubMed: 21717422]
7. Cogon D, Kellingray S, Inskip H, et al. Osteoarthritis of the Hip and Occupational Lifting. Am. J Epidemiol. 1998; 147(6):523–528. [PubMed: 9521178]
8. Felson DT, Zhang Y, Hannan MT, et al. Risk Factors For Incident Radiographic Knee Osteoarthritis In The Elderly: The Framingham Study. Arthrits Rheum. 1997; 40(4):728–733.
9. Schouten JS, van den Ouweland FA, Valkenburg HA. A 12 year follow up study in the general population on prognostic factors of cartilage loss in osteoarthritis of the knee. Ann. Rheum. Dis. 1992; 51(8):932–937. [PubMed: 1417116]
10. Buckwalter JA, Lane NE. Athletics and osteoarthritis. Occup. Heal. Ind. Med. 1998; 38(2):98.
11. Lohmander LS, Felson D. Can we identify a “high risk” patient profile to determine who will experience rapid progression of osteoarthritis? Osteoarthr. Cartil. 2004; 12:49–52.
12. Lohmander LS, Ostenberg A, Englund M, Roos H. High prevalence of knee osteoarthritis, pain, and functional limitations in female soccer players twelve years after anterior cruciate ligament injury. Arthritis Rheum. 2004; 50(10):3145–3152. [PubMed: 15476248]
13. Felson DT, Zhang Y, Anthony JM, et al. Weight Loss Reduces the Risk for Symptomatic Knee Osteoarthritis in Women. Ann. Intern. Med. 1992; 116(7):535. [PubMed: 1543306]
14. Messier SP, Loeser RF, Miller GD, et al. Exercise and dietary weight loss in overweight and obese older adults with knee osteoarthritis: the Arthritis, Diet, and Activity Promotion Trial. Arthritis Rheum. 2004; 50(5):1501–1510. [PubMed: 15146420]
15. Hochberg MC, Altman RD, April KT, et al. American College of Rheumatology 2012 recommendations for the use of nonpharmacologic and pharmacologic therapies in osteoarthritis of the hand, hip, and knee. Arthritis Care Res. 2012; 64(4):465–474.

16. Zhang Y, Jordan JM. Epidemiology of osteoarthritis. Clin. Geriatr. Med. 2010; 26(3):355–369. [PubMed: 20699159]
17. Glasson SS, Blanchet TJ, Morris EA. The surgical destabilization of the medial meniscus (DMM) model of osteoarthritis in the 129/SvEv mouse. Osteoarthr. Cartil. 2007; 15(9):1061–1069. [PubMed: 17470400]
18. Culley KL, Dragomir CL, Chang J, et al. Mouse models of osteoarthritis: surgical model of posttraumatic osteoarthritis induced by destabilization of the medial meniscus. Methods Mol. Biol. 2015; 1226:143–173. [PubMed: 25331049]
19. Kamekura S, Hoshi K, Shimoaka T, et al. Osteoarthritis development in novel experimental mouse models induced by knee joint instability. Osteoarthr. Cartil. 2005; 13(7):632–641. [PubMed: 15896985]
20. Ma H-L, Blanchet TJ, Peluso D, et al. Osteoarthritis severity is sex dependent in a surgical mouse model. Osteoarthr. Cartil. 2007; 15(6):695–700. [PubMed: 17207643]
21. Frank CB, Beveridge JE, Huebner KD, et al. Complete ACL/MCL deficiency induces variable degrees of instability in sheep with specific kinematic abnormalities correlating with degrees of early osteoarthritis. J. Orthop. Res. 2012; 30(3):384–392. [PubMed: 21919045]
22. Tashman S. Abnormal Rotational Knee Motion During Running After Anterior Cruciate Ligament Reconstruction/ Am. J. Sports Med. 2004; 32(4):975–983.
23. Tashman S, Anderst W, Kolowich P, et al. Kinematics of the ACL-deficient canine knee during gait: serial changes over two years. J. Orthop. Res. 2004; 22(5):931–941. [PubMed: 15304262]
24. Li G. In Vivo Articular Cartilage Contact Kinematics of the Knee: An Investigation Using Dual-Orthogonal Fluoroscopy and Magnetic Resonance Image-Based Computer Models. Am. J. Sports Med. 2005; 33(1):102–107. [PubMed: 15611005]
25. Allen KD, Mata BA, Gabr MA, et al. Kinematic and dynamic gait compensations resulting from knee instability in a rat model of osteoarthritis. Arthritis Res. Ther. 2012; 14(2):R78. [PubMed: 22510443]
26. Jay GD, Elsaid KA, Kelly KA, et al. Prevention of cartilage degeneration and gait asymmetry by lubricin tribosupplementation in the rat following anterior cruciate ligament transection. Arthritis Rheum. 2012; 64(4):1162–1171. [PubMed: 22127873]
27. Fritton J, Myers E, Wright T, van der Meulen M. Loading induces site-specific increases in mineral content assessed by microcomputed tomography of the mouse tibia. Bone. 2005; 36(6):1030–1038. [PubMed: 15878316]
28. De Souza RL, Matsuura M, Eckstein F, et al. Non-invasive axial loading of mouse tibiae increases cortical bone formation and modifies trabecular organization: a new model to study cortical and cancellous compartments in a single loaded element. Bone. 2005; 37(6):810–818. [PubMed: 16198164]
29. Lynch ME, Main RP, Xu Q, et al. Cancellous bone adaptation to tibial compression is not sex dependent in growing mice. J. Appl. Physiol. 2010; 109(3):685–691. [PubMed: 20576844]
30. Torrance AG, Mosley JR, Suswillo RF, Lanyon LE. Noninvasive loading of the rat ulna in vivo induces a strain-related modeling response uncomplicated by trauma or periostal pressure. Calcif. Tissue Int. 1994; 54(3):241–247. [PubMed: 8055374]
31. Mosley JR, March BM, Lynch J, Lanyon LE. Strain magnitude related changes in whole bone architecture in growing rats. Bone. 1997; 20(3):191–198. [PubMed: 9071468]
32. Lee KC, Maxwell A, Lanyon L. Validation of a technique for studying functional adaptation of the mouse ulna in response to mechanical loading. Bone. 2002; 31(3):407–412. [PubMed: 12231414]
33. Meakin LB, Price JS, Lanyon LE. The Contribution of Experimental in vivo Models to Understanding the Mechanisms of Adaptation to Mechanical Loading in Bone. Front. Endocrinol. 2014; 5:154.
34. Rubin CLL. Regulation of Bone Mass by Mechanical Strain Magnitude. Calcif. Tissue Int. 1985:411–417. [PubMed: 3930039]
35. Ko FC, Dragomir C, Plumb DA, et al. In vivo cyclic compression causes cartilage degeneration and subchondral bone changes in mouse tibiae. Arthritis Rheum. 2013; 65(6):1569–1578. [PubMed: 23436303]

36. Poulet B, Hamilton RW, Shefelbine S, Pitsillides AA. Characterizing a novel and adjustable noninvasive murine joint loading model. Arthritis Rheum. 2011; 63(1):137–147. [PubMed: 20882669]
37. Christiansen BA, Guilak F, Lockwood KA, et al. Non-invasive mouse models of post-traumatic osteoarthritis. Osteoarthr. Cartil. 2015; 23(10):1627–1638. [PubMed: 26003950]
38. Lapveteläinen T, Nevalainen T, Parkkinen JJ, et al. Lifelong moderate running training increases the incidence and severity of osteoarthritis in the knee joint of C57BL mice. Anat. Rec. 1995; 242(2):159–165. [PubMed: 7668400]
39. Selvik Gör. Roentgen stereophotogrammetry. Acta Orthop. 1989; 60(s232):1–51.
40. Valstar ER, Nelissen RGHH, Reiber JHC, Rozing PM. The use of Roentgen stereophotogrammetry to study micromotion of orthopaedic implants. ISPRS J. Photogramm. Remote Sens. 2002; 56(5–6):376–389.
41. Valstar ER, Gill R, Ryd L, et al. Guidelines for standardization of radiostereometry (RSA) of implants. Acta Orthop. 2005; 76(4):563–572. [PubMed: 16195075]
42. Wright, T., Maher, S. Potential Mechanism of PTA: Alterations in Joint Loading. In: Olsonz, S., Guilak, F., editors. Post-Traumatic Arthritis. New York: Springer; 2015.
43. Fairbank TJ. Knee Joint Changes After Meniscectomy. J Bone Jt. Surg Br. 1948; 30B(4):664–670.
44. Messner K, Gao J. The menisci of the knee joint. Anatomical and functional characteristics, and a rationale for clinical treatment. J. Anat. 1998; 193(Pt 2):161–178. [PubMed: 9827632]
45. Lee SJ, Aadalen KJ, Malaviya P, et al. Tibiofemoral contact mechanics after serial medial meniscectomies in the human cadaveric knee. Am. J. Sports Med. 2006; 34(8):1334–1344. [PubMed: 16636354]
46. Bedi A, Chen T, Santner TJ, et al. Changes in dynamic medial tibiofemoral contact mechanics and kinematics after injury of the anterior cruciate ligament: a cadaveric model. Proc. Inst. Mech. Eng. H. 2013; 227(9):1027–1037. [PubMed: 23804954]
47. Tochigi Y, Vaseenon T, Heiner AD, et al. Instability dependency of osteoarthritis development in a rabbit model of graded anterior cruciate ligament transection. J. Bone Joint Surg. Am. 2011; 93(7): 640–647. [PubMed: 21471417]
48. Fukubayashi T, Torzilli PA, Sherman MF, Warren RF. An in vitro biomechanical evaluation of anterior-posterior motion of the knee. Tibial displacement, rotation, and torque. J. Bone Joint Surg. Am. 1982; 64(2):258–264. [PubMed: 7056781]
49. Logan M. Tibiofemoral Kinematics of the Anterior Cruciate Ligament (ACL)- Deficient Weightbearing, Living Knee Employing Vertical Access Open “Interventional” Multiple Resonance Imaging. Am. J. Sports Med. 2004; 32(3):720–726. [PubMed: 15090390]
50. Iijima H, Aoyama T, Ito A, et al. Destabilization of the medial meniscus leads to subchondral bone defects and site-specific cartilage degeneration in an experimental rat model. Osteoarthr. Cartil. 2014; 22(7):1036–1043. [PubMed: 24857975]
51. Bedi A, Kelly NH, Baad M, et al. Dynamic contact mechanics of the medial meniscus as a function of radial tear, repair, and partial meniscectomy. J. Bone Joint Surg. Am. 2010; 92(6):1398–1408. [PubMed: 20516315]
52. Arunakul M, Tochigi Y, Goetz JE, et al. Replication of chronic abnormal cartilage loading by medial meniscus destabilization for modeling osteoarthritis in the rabbit knee in vivo. J. Orthop. Res. 2013; 31(10):1555–1560. [PubMed: 23843150]
53. Wright T. Biomechanical factors in osteoarthritis: the effects of joint instability. HSS J. 2012; 8(1): 15–17. [PubMed: 23372519]

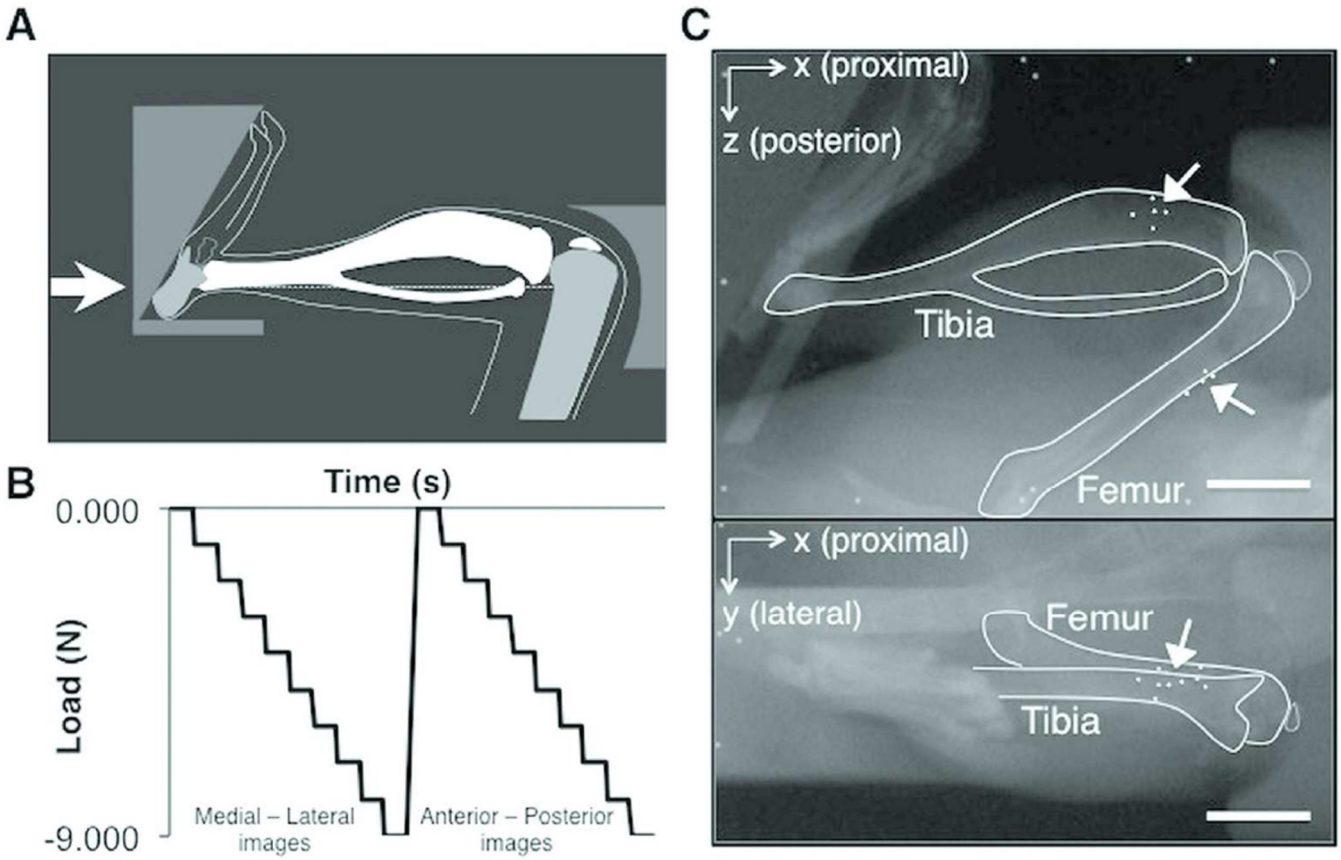

Figure 1.

(A) Schematic of the mouse tibial loading device, (B) the loading configuration for each stepped loading trial applied to the joint, and (C) radiographs of an intact joint in the loading device from 2 imaging planes, with the tibial, femoral, and bone markers outlined. Arrows indicate bone markers. Scale bar = 5.0mm

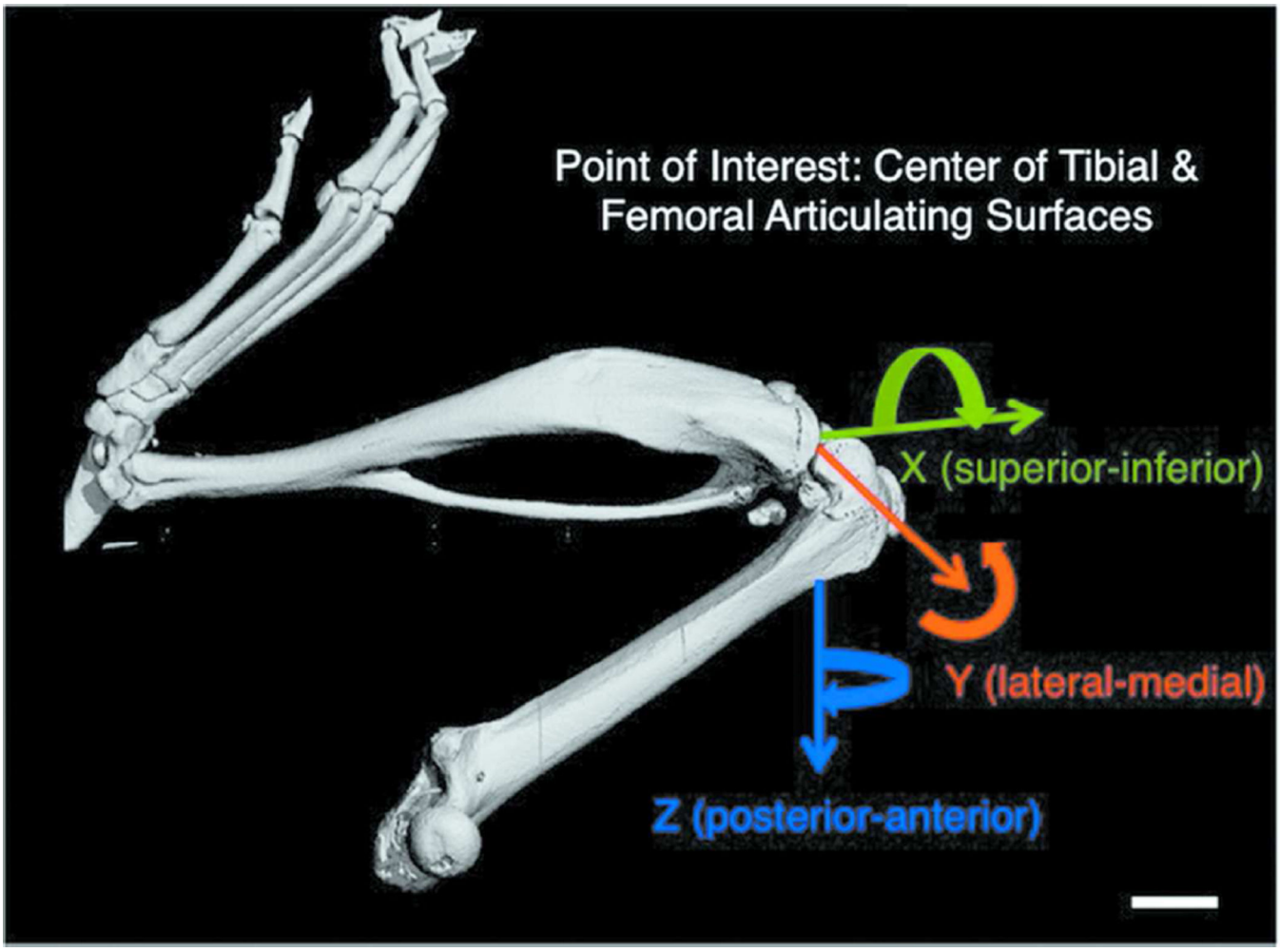

Figure 2.
Schematic of the joint axes and coordinate system relative to the tibia used for the kinematics analysis. Straight arrows indicate the Superior-Inferior axis (green), Medial-Lateral axis (red) and Posterior-Anterior axis (blue), and curved arrows indicate Internal-External (green), Flexion-Extension (red) and Adduction-Abduction (blue) rotations. Scale bar = 2.0mm

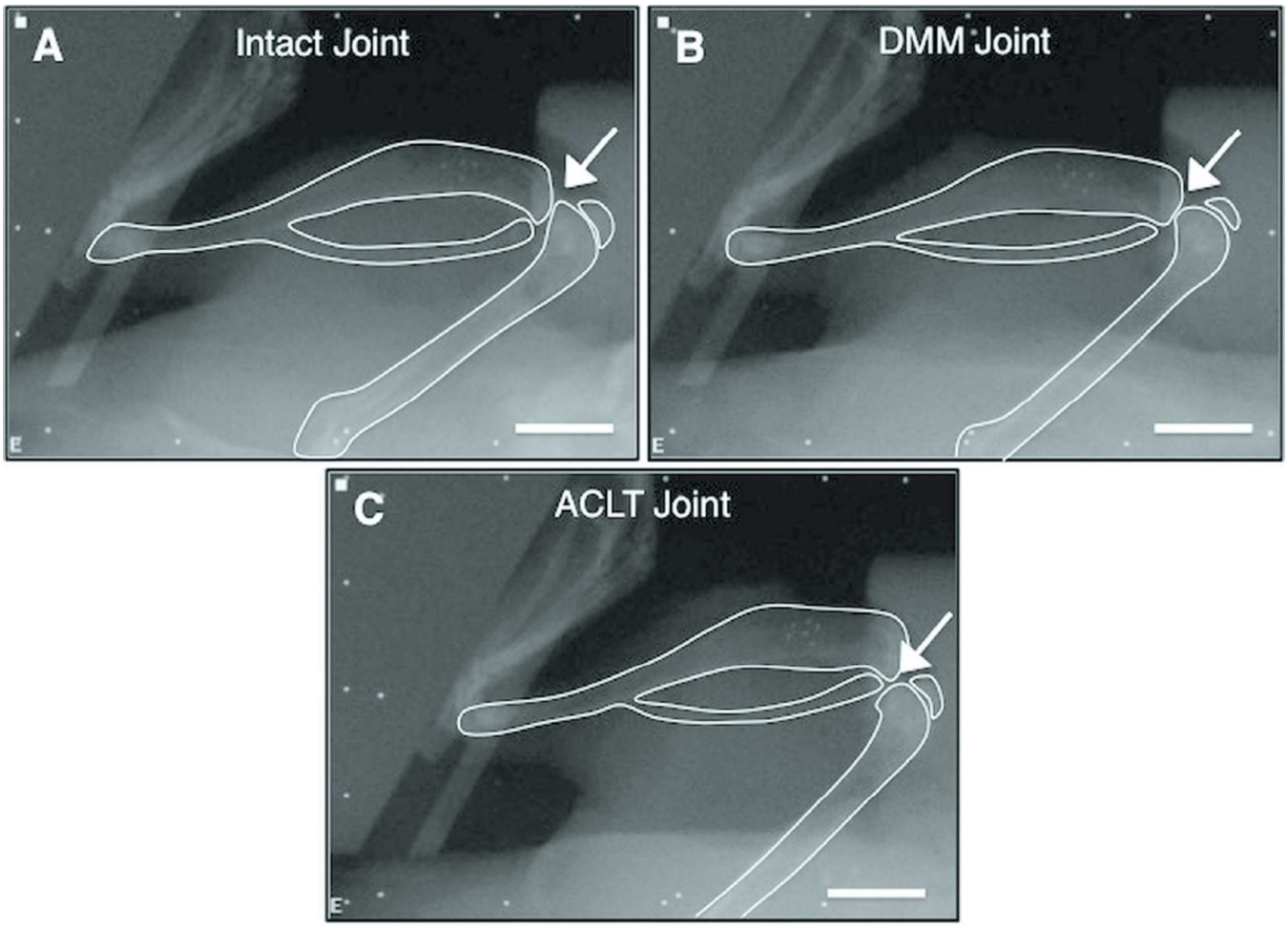

Figure 3.

Medial-lateral radiographs of an (A) intact joint (n=7), (B) DMM joint (n=4), and (C) ACLT joint (n=4) in the loading device without load. Arrows indicate articular surface. Scale bar = 5.0mm

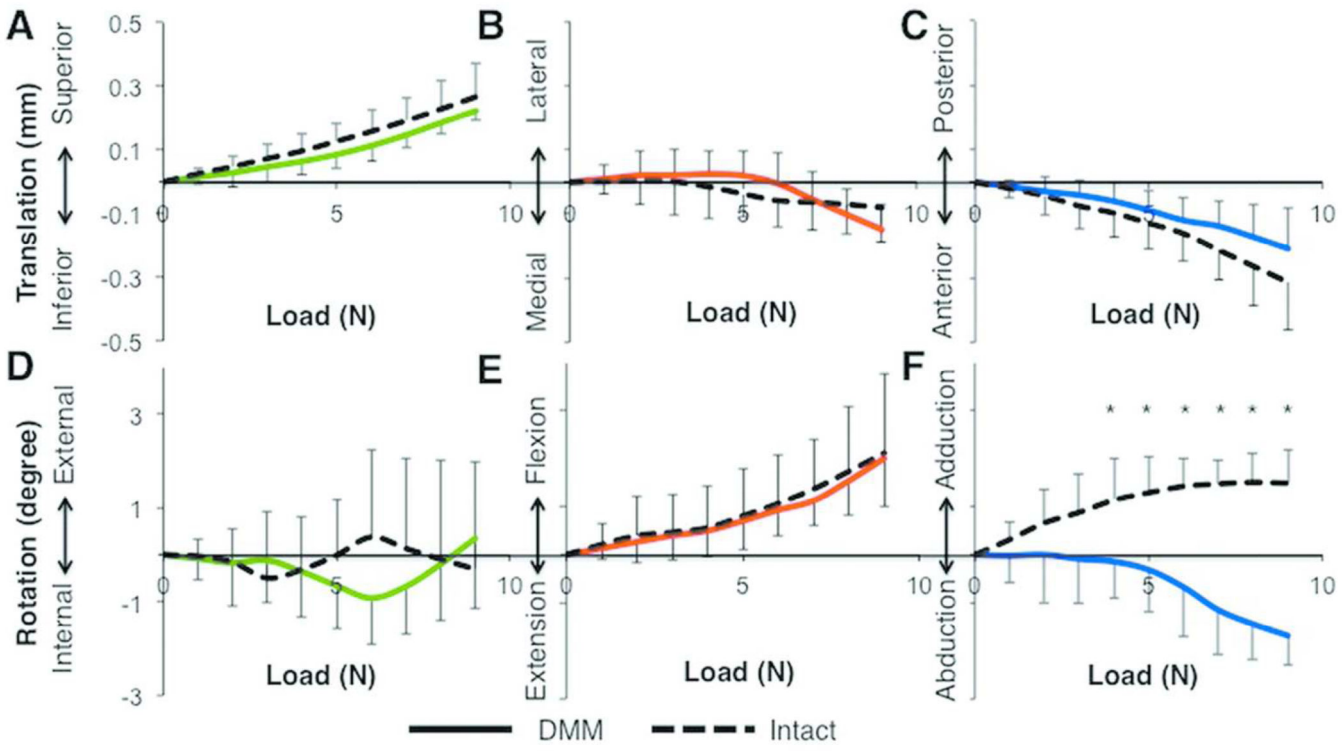

Figure 4.

Tibial translations and rotations relative to the 0N position were not different between intact (n=7) and DMM (n=4) tibiae each stepped load, except for abduction-adduction at loads greater than 3N. Data are shown for translation along the (A) Superior-Inferior, (B) Lateral-Medial, and (C) Posterior-Anterior axes, and (D) Internal-External, (E) Flexion-Extension, and (F) Adduction-Abduction rotation. Data colors correspond to axis colors in Figure 2. *, $p<0.05$ by Kruskal-Wallis test.

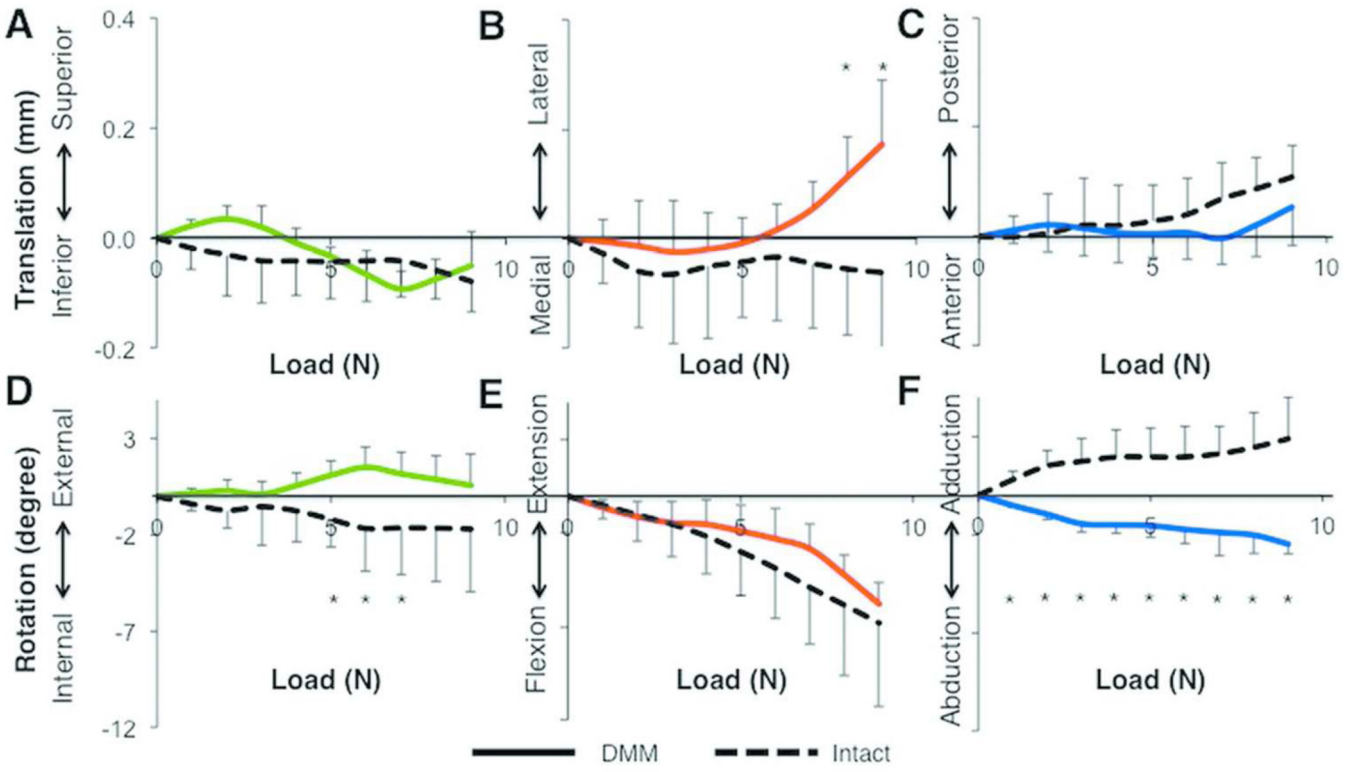

Figure 5.

Most relative femur-to-tibia translations and rotations were not different between intact (n=7) and DMM (n=4) tibiae at each stepped load, except for translation along the medial-lateral axis at 8 and 9N and rotation about the anterior-posterior axis. Data are shown for translation along the (A) Superior-Inferior, (B) Lateral-Medial, and (C) Posterior-Anterior axes, and (D) Internal-External, (E) Flexion-Extension, and (F) Adduction-Abduction rotation. Data colors correspond to axis colors in Figure 2. *, $p<0.05$ by Kruskal-Wallis test.